RSC Advances

PAPER

View Article Online
View Journal | View Issue

Cite this: *RSC Adv.*, 2020, **10**, 31889

Porous lithium cobalt oxide fabricated from metal–organic frameworks as a high-rate cathode for lithium-ion batteries†

Hao Wei,[a] Yuan Tian,[a] Yongling An,[a] Jinkui Feng,*[a] Shenglin Xiong[b] and Yitai Qian[b]

Received 27th June 2020
Accepted 16th August 2020

DOI: 10.1039/d0ra05615d

rsc.li/rsc-advances

Porous materials have many applications, such as energy storage, as catalysts and adsorption *etc.* Nevertheless, facile synthesis of porous materials remains a challenge. In this work, porous lithium cobalt oxide ($LiCoO_2$) is fabricated directly from Co-based metal–organic frameworks (MOFs, ZIF-67) and lithium salt *via* a facile solid state annealing approach. The temperature affect on the microstructure of $LiCoO_2$ is also investigated. The as-prepared $LiCoO_2$ shows a uniform porous structure. As a cathode for a lithium-ion battery (LIB), the $LiCoO_2$ delivers excellent stability and superior rate capability. The as-prepared porous $LiCoO_2$ delivers a reversible capacity of 106.5 mA h g^{-1} at 2C and with stable capacity retention of 96.4% even after 100 cycles. This work may provide an alternative pathway for the preparation of porous materials with broader applications.

1. Introduction

Owing to their special 3D structure, porous materials play an important role in energy storage, catalysis, adsorption and many other fields.[1–3] The lack of a facile preparation route for porous materials is one of the key restrictions for their wide application. Various methods have been developed to obtain porous materials, such as the template method, sol–gel and dealloying *etc.*[4,5] However, facile fabrication of porous materials remains a great challenge.

The lithium-ion battery (LIB) is one of the most promising power sources for electronics and electric vehicles.[6] $LiCoO_2$, as one of the most successful cathode materials for LIBs, and has always been promising in the field since the commercialization of LIBs, as it has the advantages of high working potential, high specific capacity and good cycling performance *etc.*[7,8]

With the fast development of electronics such as drones, 5G, and electric vehicles, the high rate performance of LIBs becomes an essential property. Great interest and effort has been devoted to improving the rate performance of LIBs. One promising strategy is regulating the cathode structure to become porous. The porous structure could shorten the transport distance of ions, increase the contact between electrode and electrolyte, and buffer the volume expansion.[9,10] Porous structured $LiCoO_2$ has been prepared by various methods, such as Li-vapor crystal growth, template synthesis, electrostatic spray deposition, *etc.*, and has proven to improve rate performance.[11–13] For example, Mitsunori Kitta *et al.* obtained the porous $LiCoO_2$ crystal film on the CoO substrate surface by the Li-vapor crystal growth method.[14] Ghamouss Fouad *et al.* prepared a porous $LiCoO_2$ cathode *via* electrospray deposition.[15] Nevertheless, the synthesis of porous $LiCoO_2$ with a facile method still needs further exploration.

The metal–organic framework (MOF) is an emerging kind of porous coordination polymer, which is composed of organic ligands and inorganic moieties. MOFs possess the characteristics of large pore volume and larger surface area. Moreover, the synthesis of MOFs is relatively facile and scalable.[16–18] A number of studies in recent years indicate that MOFs could serve as precursors to obtain porous materials.[19,20] For example, Yuanyuan Liu *et al.* have obtained a porous lithium iron phosphate ($LiFePO_4$) composite cathode from an Fe based metal–organic framework (MIL-100 (Fe)).[19] The intrinsically porous architecture of MOFs could remain in the final products.

In this work, taking $LiCoO_2$ as an example, a porous oxide-based cathode can be successfully fabricated using Co-based MOFs (ZIF-67) as a precursor *via* a facile annealing approach. Porous $LiCoO_2$ may provide more contact sites, shorten the pathway of the Li-ion transport, and reduce the negative impact of the volume expansion during high rate charge–discharge. The idea may be extended to the synthesis of other porous alkali metal cathode materials such as lithium manganese oxide, sodium cobalt oxide, and potassium manganese oxide *etc.*

[a]*Key Laboratory for Liquid-Solid Structural Evolution & Processing of Materials (Ministry of Education), School of Materials Science and Engineering, China. E-mail: jinkui@sdu.edu.cn*

[b]*School of Chemistry and Chemical Engineering, Shandong University, Jinan 250061, China*

† Electronic supplementary information (ESI) available. See DOI: 10.1039/d0ra05615d

2. Experimental section

ZIF-67 was synthesized by a solution method based on a previous report.[21] All of the reagents were purchased and used without further purification. For the typical synthesis of ZIF-67, 1.45 g cobalt hexahydrate nitrate ($Co(NO_3)_2 \cdot 6H_2O$, 99%, Aladdin) and 40 mg cetyltrimethylammonium bromide (CTAB, 90%, Aladdin) were dissolved in 50 mL water to obtain a uniform solution. The solution was rapidly injected into a 350 mL aqueous solution containing 22.7 g 2-methylimidazole (98%, Aladdin). Then the mixture was stirred for another 30 min, and the precipitate was collected by filtering and drying in an oven at 80 °C until a blue color was obtained. For the preparation of $LiCoO_2$, the prepared ZIF-67 was ground for 1 h with lithium hydroxide monohydrate ($LiOH \cdot H_2O$, 98%, Aladdin) (Co/Li 1.0 : 1.02 mol/mol). Then the mixture was heated to 650 °C, 700 °C and 750 °C in the air atmosphere at a rate of 2 °C min^{-1}. Then the mixture was kept at the top temperature for 2 h. The obtained $LiCoO_2$ is black (Fig. S1†). The commercial $LiCoO_2$ is bought from Sigma-Aldrich.

Crystal structures were characterized *via* X-ray diffraction (XRD, Rigaku Dmaxrc diffractometer) using Cu-Kα radiation between 5° and 90° with a scan rate of 10° min^{-1}. The morphologies and microstructures were measured *via* scanning electron microscopy (SEM, SU-70) and high-resolution transmission electron microscopy (HR-TEM JEM-2100). The surface area and pore distribution of the as-synthesized samples were estimated by Brunauer–Emmett–Teller theory (BET, ASAP 2020) based on N_2 adsorption.

To test the electrochemical performance, the as-synthesized porous $LiCoO_2$ was mixed with Super P and polyvinylidene fluoride (PVDF) (8 : 1 : 1 by mass) in NMP for 12 h to obtain a homogeneous slurry. The cathode electrode was prepared by casting it on aluminum foil and drying in a vacuum oven at 80 °C for 24 h. The loading of electrode was about 2 mg cm^{-2}. The solute of the electrolyte was 1 M lithium hexafluorophosphate in ethylene carbonate and diethyl carbonate (EC and DEC, volume ratio 1 : 1) with 5 wt% fluoroethylene carbonate (FEC). The counter and reference electrode were both lithium foil. The commercial $LiCoO_2$ (99%, Aladdin) electrode was also prepared in the same way. The cell was assembled in the vacuum glove box (Mikrouna Super 1220/750) with water and oxygen content lower than 1 ppm. The electrochemical performance was tested. Cyclic voltammetry (CV) was tested on the electrochemical workstation (CHI660E), and the discharge/charge performance was tested on charge–discharge equipment (Neware) between 3 and 4.2 V at different current densities.

3. Results and discussion

The synthesis process of porous $LiCoO_2$ is simulated in Scheme 1. The ZIF-67 and $LiOH \cdot H_2O$ were simply mixed by grinding and heating to 650 °C, 700 °C and 750 °C for 2 h to obtain $LiCoO_2$. It can be predicted that the temperature will inevitably affect the solid-state reaction, which can affect the detailed structure of the porous products.

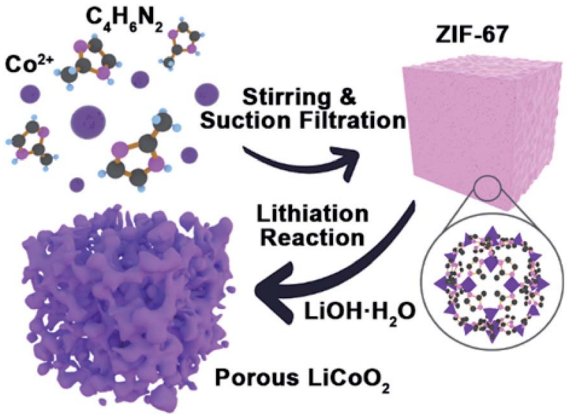

Scheme 1 The synthesis of nanoporous $LiCoO_2$.

The indexed XRD patterns of the ZIF-67 precursor and as-obtained $LiCoO_2$ are shown in Fig. 1a and b. From the figures, we can see that the XRD pattern of the as-prepared ZIF-67 and $LiCoO_2$ are consistent with the previous reports and standard $LiCoO_2$ patterns (JCPDS card no. 75-0532), which indicates that $LiCoO_2$ can be successfully synthesized from ZIF-67.[21,22] BET tests were performed to measure the surface area and pore size distribution of the as-prepared $LiCoO_2$ (Fig. 1c and d). The as-prepared $LiCoO_2$ had an average pore diameter of 7.5 nm and a surface area of around 9.2 m^2 g^{-1}. The larger specific surface area and rich pores are beneficial for Li-ion transport, which could benefit the rate performance.[23] At the same time, the moderate surface area increase can balance the ion transport and side reactions due to the larger surface area.

The morphology and microstructure of the as-prepared ZIF-67 and $LiCoO_2$ were further probed *via* SEM and HR-TEM. SEM photographs of the ZIF-67 at different magnifications are shown in Fig. 2a and b. The ZIF-67 displays a uniform cubic shape with

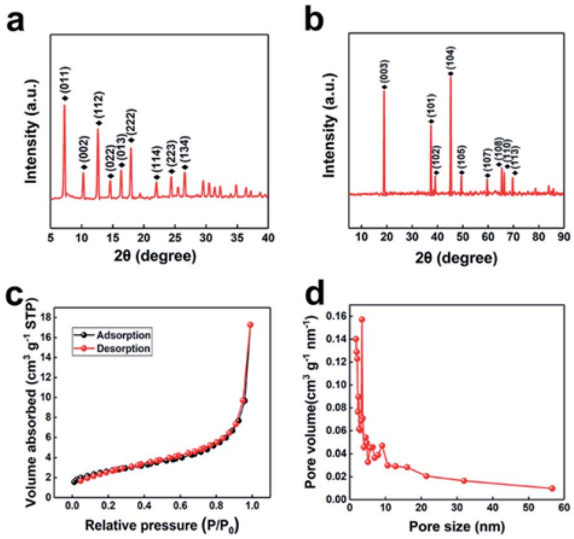

Fig. 1 XRD patterns of (a) ZIF-67 and (b) porous $LiCoO_2$, BET of (c) surface area and (d) the pore size distribution of the porous $LiCoO_2$.

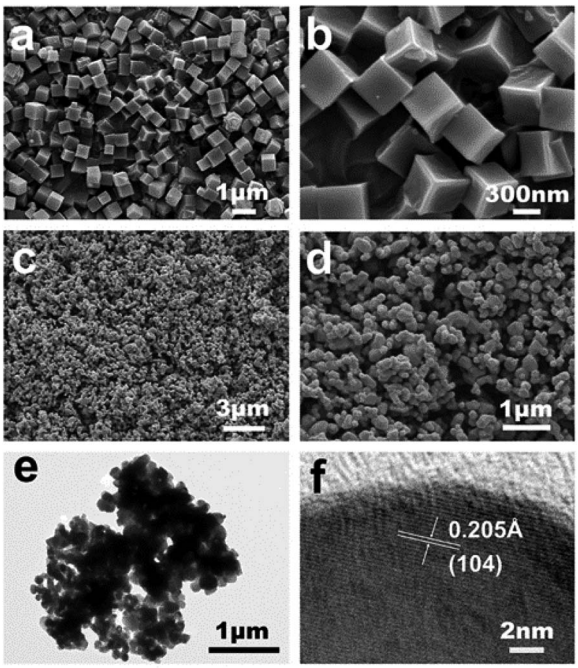

Fig. 2 SEM micrographs of (a and b) ZIF-67 (Co) and (c and d) porous $LiCoO_2$ at different magnifications, (e) TEM micrograph and (f) HR-TEM micrograph of porous $LiCoO_2$.

an edge length of around 450 nm, which is consistent with previous reports.[21] Fig. 2c and d show SEM images of the as-prepared 700 °C $LiCoO_2$ sample. From the figures we can see that the particle size of the as-prepared $LiCoO_2$ is distributed in the range 200–300 nm. The TEM investigation confirms that the as-prepared $LiCoO_2$ is porous (Fig. 2e). From the figure we can see that the 3D porous framework is formed by inter-connected tiny $LiCoO_2$ crystals. The structure could increase the charge transfer between the electrolyte and electrode with good bulk ion transport rate, and shorten the ion transport in the electrode.[24] In contrast, the SEM and TEM images of $LiCoO_2$ prepared at 650 °C and 750 °C are also given in Fig. S2–S5.† From the figures (Fig. S2†) we can see that at 650 °C, the as-prepared $LiCoO_2$ has inhomogeneous size and pore distribution. Moreover, from the HR-TEM (Fig. S3†) we can see that the 650 °C $LiCoO_2$ is poorly crystallized, which suggested that 650 °C is not sufficient for the synthesis of well-crystallized $LiCoO_2$. For the $LiCoO_2$ prepared at 750 °C, an aggregated morphology is observed with a smaller pore volume (Fig. S4 and S5†), which suggested that 750 °C is too high for the preparation of porous $LiCoO_2$. This may be due to the swelling of the porous structure when the annealing temperature is higher. A smaller pore volume is not beneficial for lithium ion transport. Fig. 2f shows the HR-TEM images of the as-prepared 700 °C $LiCoO_2$, the lattice constant is consistent with standard $LiCoO_2$. A proper crystal structure of the cathode material is essential for the excellent electrochemical properties. Too high or too low may deteriorate the pore and crystalline structure of $LiCoO_2$. Furthermore, the $LiCoO_2$ electrode after cycling was investigated. It can be seen that no significant change is observed in morphology (Fig. S7†). The porous structure of $LiCoO_2$ remained, which verified that the structure is stable during cycling.

The electrochemical properties of as-prepared $LiCoO_2$ were further examined by CV and static current charge–discharge. For the CV measurement, the $LiCoO_2$ electrode was cycled at a scan rate of 0.5 mV s^{-1} between 3 V and 4.2 V (Fig. 3a). As we can see, a pair of reversible peaks owing to lithium intercalation and deintercalation in the layered $LiCoO_2$, appeared at 4.15 and 3.75 V, which is typical for $LiCoO_2$. The subsequent curves almost overlap, which implied the high reversibility of the as-prepared porous $LiCoO_2$. The first 10 cycles of charge–discharge curves of $LiCoO_2$ are presented in Fig. 3b at 0.5C, from the figure we can see that the curves almost overlap, confirming the good cycling ability of $LiCoO_2$. Fig. 3c shows the cyclability of the porous and commercial $LiCoO_2$ electrode at a low rate (2C). The porous $LiCoO_2$ shows a higher capacity with similar capacity retention at 2C. The rate performance was further studied in detail to characterize the rate capability of the as-prepared porous $LiCoO_2$, and the results are shown in Fig. 3d. As we initially expected, with increased current density, the porous $LiCoO_2$ delivers reversible capacities of 123 mA h g^{-1}, 120 mA h g^{-1}, 118 mA h g^{-1}, 110 mA h g^{-1}, 102 mA h g^{-1}, 96 mA h g^{-1}, 89 mA h g^{-1}, and 79 mA h g^{-1} at a current density of 0.5, 1, 2, 3, 4, 5, 6, and 7C, respectively. For commercial $LiCoO_2$, the capacity rapidly decreased as the

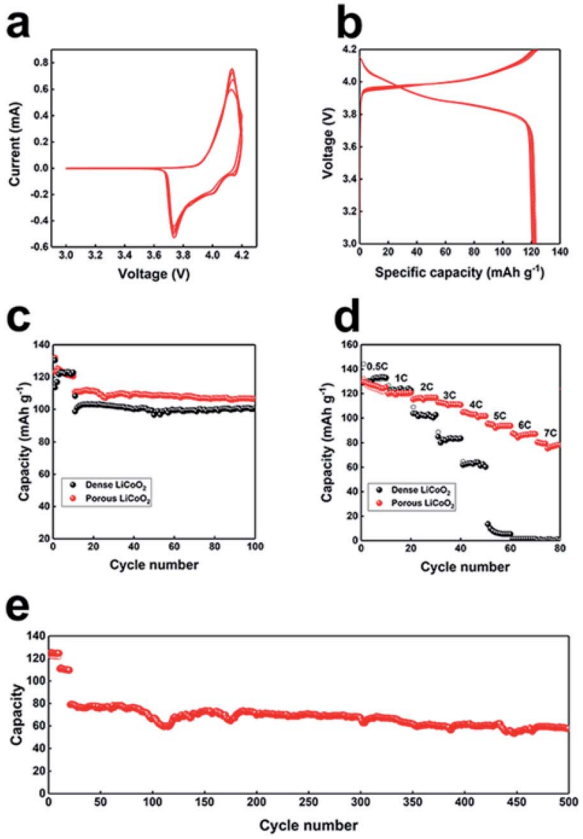

Fig. 3 (a) 1–5th cyclic voltammograms of porous $LiCoO_2$. (b) 1–10th charge–discharge profiles of porous $LiCoO_2$. (c) Capacity *vs.* cycle number for porous and commercial $LiCoO_2$ at 2C. (d) The capacity of porous $LiCoO_2$ at different rates. (e) Cycling performance of porous $LiCoO_2$ at 5C.

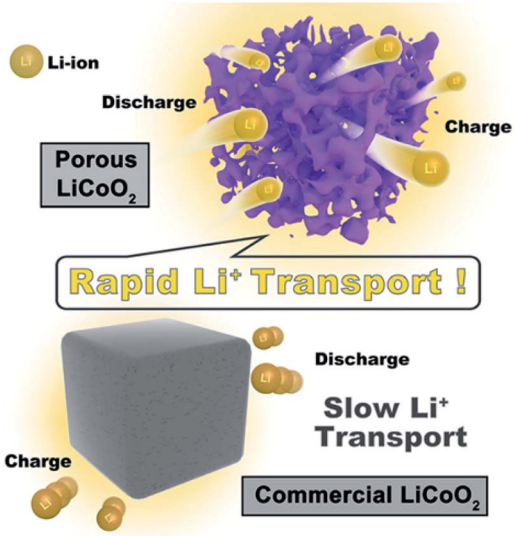

Scheme 2 The high rate mechanism of the $LiCoO_2$ cathode.

current density increased. When the current density was 6C, the capacity of commercial $LiCoO_2$ reduced to nearly 0. The superior rate performance may be ascribed to the porous structure of aggregated nanosized $LiCoO_2$ crystals, which ensures a faster charge transfer rate between the electrolyte–electrode and higher ion transport due to the lower ion transport pathway.[11–13] Moreover, the porous $LiCoO_2$ electrode also presented a stable long-cycling performance (Fig. 3e) with a capacity retention of 70% even after 500 cycles. The good reversibility implies the stable porous structure of the as-prepared $LiCoO_2$. The charge–discharge profiles at different rate and cycling number are also given (Fig. S6†), from the figure we can see that the voltage profiles are almost the same at a different rate and cycling number, which further confirms the stable structure of the as-prepared $LiCoO_2$.[11–13] In addition, the electrochemical performance of the as-synthesized porous $LiCoO_2$ is compared with previously reported work (Table S1†). By comparison, it can be found that the porous $LiCoO_2$ cathode has outstanding performance in terms of rate, cycling stability and reversible capacity.

Scheme 2 shows the high rate mechanism of the as-prepared porous $LiCoO_2$ materials. Obviously, the main difference between porous $LiCoO_2$ and commercial $LiCoO_2$ is the robust 3D porous structure, which provides better electrode/electrolyte contact sites to promote charge transfer. Moreover, the special pore structure could shorten the ion transport, which benefits the lithium ion diffusion. Finally, the robust 3D porous structure can reduce the negative impact of the volume changes of $LiCoO_2$ during Li-ion intercalation and de-intercalation at high rates, which would cause the crystal collapse.[25–27] The results may be useful for developing other high rate materials.

4. Conclusions

In conclusion, uniform porous $LiCoO_2$ is successfully synthesized with ZIF-67 and lithium salt at 700 °C in 2 h *via* a simple solid method. The direct utilization of nanosize MOF as a precursor is one of the key merits of this work, which is different from the traditional preparation process for $LiCoO_2$. During the annealing process, the rich porous structure of the precursor is retained, which provides the superior porous structure of as prepared $LiCoO_2$. Moreover, the organic ligand is oxidized to form gases such as water vapor and carbon oxides at a high temperature, which can help pore formation. Additionally, the solid state synthesis process is easier than commercial production. By ensuring faster charge transfer between the electrolyte–electrode, and higher ion transport due to the lower ion transport pathway and robust 3D structure, the porous $LiCoO_2$ electrode exhibits outstanding rate performance and long cycling ability. The high cost of MOF may be a limitation, however, the promising rate performance may enable it to be utilized in special areas. This work may also be useful for the design of other high performance energy storage materials and other functional materials.

Conflicts of interest

There are no conflicts to declare.

Acknowledgements

This work was supported by the State Key Program of National Natural Science of China (61633015), the National Natural Science Foundation of China (51972198), Taishan Scholars Program of Shandong Province, the Project of the Taishan Scholar (ts201511004, tsqn201812002, ts20190908), and the Young Scholars Program of Shandong University (2016WLJH03).

References

1 Y. Cheng, Y. Ying, J. Susilo, S. Jiang, T. Chung, S. Zhang and D. Zhao, *Adv. Mater.*, 2018, **47**, 1802401.
2 S. Das, P. Heasman, T. Ben and S. Qiu, *Chem. Rev.*, 2017, **117**, 1515–1563.
3 J. Liang, Z. Liang, R. Zou and Y. Zhao, *Adv. Mater.*, 2017, **29**, 1701139.
4 A. Fu, C. Wang, F. Pei, J. Cui, X. Fang and N. Zheng, *Small*, 2019, **15**, 1804786.
5 Z. Liu, X. Yuan, S. Zhang, J. Wang, Q. Huang, N. Yu, Y. Zhu, L. Fu, F. Wang, Y. Chen and Y. Wu, *NPG Asia Mater.*, 2019, **11**, 12.
6 M. Li, J. Lu, Z. Chen and K. Amine, *Adv. Mater.*, 2018, **30**, 1800561.
7 J. P. Brog, A. Crochet, J. Seydoux, M. J. D. Clift, B. Baichette, S. Maharajan, H. Barosova, P. Brodard, M. Spodaryk, A. Züttel, B. R. Rutishauser, N. H. Kwon and K. M. Fromm, *J. Nanobiotechnol.*, 2017, **15**, 58.
8 Z. Tian, H. Yu, Z. Zhang and X. Xu, *ChemBioEng Rev.*, 2018, **5**, 111–118.
9 M. K. Shobana and Y. Kim, *J. Alloys Compd.*, 2017, **729**, 463–474.
10 J. Liu, J. Long, S. Du, B. Sun, S. Zhu and J. Li, *Nanomaterials*, 2019, **9**, 441.

11 G. Saat, F. M. Balci, E. P. Alsaç, F. Karadas and Ö Dag, *Small*, 2018, **14**, 1701913.
12 J. Xie, J. Zhao, Y. Liu, H. Wang, C. Liu, T. Wu, P. Hsu, D. Lin, Y. Jin and Y. Cui, *Nano Res.*, 2017, **10**, 3754–3764.
13 L. Xue, S. V. Savilov, V. V. Lunin and H. Xia, *Adv. Funct. Mater.*, 2018, **28**, 1705836.
14 M. Kitta and K. Kuratani, *Cryst. Growth Des.*, 2019, **19**, 150–156.
15 I. Bezza, E. Luais, F. Ghamouss, M. Zaghrioui, F. Tran-van and J. Sakai, *J. Alloys Compd.*, 2019, **805**, 19–25.
16 Y. V. Kaneti, S. Dutta, M. S. A. Hossain, M. J. A. Shiddiky, K. L. Tung, F. K. Shieh, C. K. Tsung, C. W. Wu and Y. Yamauchi, *Adv. Mater.*, 2017, **29**, 1700213.
17 Y. An, H. Fei, Z. Zhang, L. Ci, S. Xiong and J. Feng, *Chem. Commun.*, 2017, **53**, 8360.
18 Y. Xue, S. Zheng, H. Xue and H. Pang, *J. Mater. Chem. A*, 2019, **7**, 7301.
19 Y. Liu, J. Gu, J. Zhang, F. Yu, L. Dong, N. Nie and W. Li, *J. Power Sources*, 2016, **304**, 42–50.
20 J. Li, H. Zhao, J. Wang, N. Li, M. Wu, Q. Zhang and Y. Du, *Nano Energy*, 2019, **62**, 876–882.
21 S. K. Parka, J. K. Kima, J. H. Kimb and Y. C. Kang, *Mater. Charact.*, 2017, **132**, 320.
22 X. Yang, J. Chen, Y. Chen, P. Feng, H. Lai, J. Li and X. Luo, *Nano-Micro Lett.*, 2018, **10**, 15.
23 J. Huang, W. Wang, X. Lin, C. Gu and J. Liu, *J. Power Sources*, 2018, **378**, 677–684.
24 Z. Li, X. Feng, L. Mi, J. Zheng, X. Chen and W. Chen, *Nano Res.*, 2018, **11**, 4038–4048.
25 Q. Liu, M. S. Javed, C. Zhang, Y. Li, C. Hu, C. Zhang, M. Lai and Q. Yang, *Nanoscale*, 2017, **9**, 5509.
26 H. Meng, L. Li, J. Liu, X. Han, W. Zhang, X. Liu and Q. Xu, *J. Alloys Compd.*, 2017, **690**, 256–266.
27 S. Zhang, X. Li, B. Ding, H. Li, X. Liu and Q. Xu, *J. Alloys Compd.*, 2020, **822**, 153624.